Virology 452-453 (2014) 75–85

Contents lists available at ScienceDirect

Virology

journal homepage: www.elsevier.com/locate/yviro

KSHV cell attachment sites revealed by ultra sensitive tyramide signal amplification (TSA) localize to membrane microdomains that are up-regulated on mitotic cells

H. Jacques Garrigues [a], Yelena E. Rubinchikova [a], Timothy M. Rose [a,b,*]

[a] Seattle Children's Research Institute, 1900 Ninth Ave, 8th Floor, Seattle, WA 98101, USA
[b] University of Washington, Seattle, WA 98195, USA

ARTICLE INFO

Article history:
Received 18 October 2013
Returned to author for revisions
28 November 2013
Accepted 7 January 2014
Available online 31 January 2014

Keywords:
Kaposi's sarcoma-associated herpesvirus (KSHV)
Human herpesvirus 8 (HHV8)
Mitosis
Tyramide signal amplification (TSA)
Attachment
Binding site
Confocal microscopy

ABSTRACT

Cell surface structures initiating attachment of Kaposi's sarcoma-associated herpesvirus (KSHV) were characterized using purified hapten-labeled virions visualized by confocal microscopy with a sensitive fluorescent enhancement using tyramide signal amplification (TSA). KSHV attachment sites were present in specific cellular domains, including actin-based filopodia, lamellipodia, ruffled membranes, microvilli and intercellular junctions. Isolated microdomains were identified on the dorsal surface, which were heterogeneous in size with a variable distribution that depended on cellular confluence and cell cycle stage. KSHV binding domains ranged from scarce on interphase cells to dense and continuous on mitotic cells, and quantitation of bound virus revealed a significant increase on mitotic compared to interphase cells. KSHV also bound to a supranuclear domain that was distinct from microdomains in confluent and interphase cells. These results suggest that rearrangement of the cellular membrane during mitosis induces changes in cell surface receptors implicated in the initial attachment stage of KSHV entry.

Introduction

The Kaposi's sarcoma-associated herpesvirus/human herpesvirus 8 (KSHV) is the causative agent of Kaposi's sarcoma, pleural effusion lymphoma and multicentric Castleman's disease (Ganem, 2006). In vitro, KSHV infects a broad spectrum of cells, including lymphocytic, endothelial, epithelial and mesenchymal cells (Bechtel et al., 2003; Lagunoff et al., 2002). Initiation of the infectious process of KSHV and other herpesviruses is believed to involve the attachment to heparan sulfate (HS), which is ubiquitously expressed on proteoglycans at the cell surface (Akula et al., 2001b; Birkmann et al., 2001; Liu and Thorp, 2002). Several KSHV virion proteins bind HS, including glycoprotein B (Akula et al., 2001a), K8.1 (Birkmann et al., 2001; Wang et al., 2001), glycoprotein H (Hahn et al., 2009) and complement control protein (KCP) (Mark et al., 2006). Enzymatic removal of cell surface HS results in reduced susceptibility of target cells to KSHV infection (Akula et al., 2001b), and cells that express low levels of HS are resistant to KSHV infection (Jarousse et al., 2008). Virion interactions with HS proteoglycans are believed to concentrate virus on cell surface domains to promote virus entry through additional cell surface entry receptors. Several cell surface proteins have been implicated as KSHV entry receptors, including DC-SIGN (Rappocciolo et al., 2008; Rappocciolo et al., 2006), the cystine transporter (xCT) light chain (Kaleeba and Berger, 2006) and CD98 heavy chain heterodimer (Veettil et al., 2008), the ephrin receptor tyrosine kinase A2 (EphA2)(Hahn et al., 2012), syndecan (Hahn et al., 2009, 2012), and the integrins $\alpha3\beta1$, $\alpha v\beta3$ and $\alpha v\beta5$ (Akula et al., 2002; Garrigues et al., 2008; Veettil et al., 2008).

Previous studies have focused on KSHV/receptor interactions occurring after initial virus contact with the plasma membrane. Time-dependent translocation of KSHV into lipid rafts along with $\alpha v\beta3$ and $\alpha3\beta1$ integrins and xCT receptors was observed in endothelial cells (Veettil et al., 2008). However, there is limited morphological data correlating the position of cell surface bound KSHV with the distribution of HS or other entry receptors at initial attachment sites before virus entry.

Advances in fluorescence technologies coupled with confocal microscopy have provided novel approaches to visualize viruses and their interaction with cell surfaces. Virion particles have been

* Corresponding author at: Seattle Children's Research Institute, 1900 9th Avenue, 8th Floor, Seattle, WA 98101, USA. Tel.: +1 206 884 8229; fax: +1 206 884 7311.
E-mail addresses: Jacques.garrigues@seattlechildrens.org (H.J. Garrigues), yrubinchikova@pnwu.edu (Y.E. Rubinchikova), timothy.rose@seattlechildrens.org, trose@u.washington.edu (T.M. Rose).

0042-6822/$ - see front matter © 2014 Elsevier Inc. All rights reserved.
http://dx.doi.org/10.1016/j.virol.2014.01.006

labeled using a variety of different approaches, including incorporation of exogenous fluorescent proteins, such as green fluorescent protein (GFP), as fusions with virion structural proteins, or incorporation of fluorescent dyes in the lipid virion envelope membrane (Balogh et al., 2011). Indirect fluorescent techniques utilize the incorporation of small peptide tags, such as tetracysteine, fused in-frame with virion proteins (Whitt and Mire, 2011) or chemical labeling of virion proteins using small haptens with the addition of fluorophores that covalently or non-covalently interact with the modified proteins. While all of these approaches have been utilized to visualize virus interactions with cell surfaces, each is associated with potential problems of sensitivity and specificity of detection and efficiency and ease of labeling.

To identify KSHV plasma membrane binding domains, we developed and optimized a highly sensitive technique to visualize hapten-labeled KSHV virions bound to target cells using confocal fluorescence microscopy with tyramide signal amplification (TSA) and 3D-surface rendering. The TSA enhancement technique was 500 fold more sensitive than conventional immunofluorescence, and allowed us to identify specific cell surface microdomains that bind KSHV during the initial attachment phase of infection. The distribution of KSHV binding microdomains was dependent on cell density in confluent and sub-confluent cultures, and increased binding was detected on mitotic cells. The characterization of the KSHV attachment domains along with improved virus detection will allow us to determine if HS or other proposed entry receptors are present in KSHV microdomains and determine whether the increased binding of mitotic cells correlates with a particular receptor constitution within the KSHV microdomains.

Results

Purification of hapten-labeled infectious KSHV virions

In order to characterize cell membrane domains that mediate the initial attachment and entry of KSHV, we developed a highly sensitive tyramide signal amplification (TSA) method to visualize cell bound hapten-labeled virus. KSHV virions from culture supernatants of TPA treated KSHV infected BCBL-1 cells were labeled with the hapten dinitrophenol (DNP) and subsequently purified on an Opti-Prep step gradient, as described previously (Garrigues et al., 2008). PCR analysis of gradient fractions identified a major peak of labeled KSHV in fractions 10 and 11 (Fig. 1A). Selected fractions (5, 7, 9, 11, 13, and 15) were screened for the presence of infectious virus using Vero cells as target, and the percent of infected cells expressing the KSHV ORF73 latency-associated nuclear antigen (LANA), a marker of KSHV latent infection, was determined, as described in Materials and methods. The major peak of viral DNA, fraction 11 was highly infectious in comparison to the other tested fractions (Fig. 1A).

To determine if hapten incorporation altered KSHV infectivity, gradient purified KSHV virions were labeled with increasing concentrations of DNP or biotin. The labeled virus was purified from unincorporated hapten and used to infect Vero cells. The percent of infected cells was determined by staining for LANA expression. Hapten concentrations up to 50 μg/ml of DNP or biotin did not significantly affect KSHV infectivity when compared to control unlabeled virus (Fig. 1B). A hapten concentration of 10 μg/ml was chosen for labeling KSHV virions for the remainder of the study.

Our initial attempts to visualize the distribution of cell bound DNP-KSHV using anti-DNP in combination with FITC labeled secondary antibodies were unsuccessful due to the low sensitivity of this unamplified fluorescent technique. For this reason we investigated a signal amplification technique using fluorescent tyramide.

Tyramide signal amplification enhances the sensitivity of KSHV detection

Tyramide signal amplification (TSA) is an enzyme mediated detection method reported to be a 100-fold more sensitive than conventional fluorescent methods (Bobrow et al., 1989; Speel et al., 1999). TSA enhancement is achieved with an antibody coupled to horse radish peroxidase (HRP), which catalyzes the activation of fluorescent tyramide that becomes covalently linked to tyrosine residues in proteins at the site of the localized HRP-antibody. Our initial assessment was done using an indirect immunoassay with biotinylated IgG coupled to magnetic beads. The beads were incubated with mouse anti-biotin IgG and dilutions of goat anti-mouse IgG conjugated with either HRP or FITC. The FITC fluorescence was measured directly while the HRP activity was detected using signal enhancement with TSA488. A strong fluorescent TSA signal (113.8 ± 15 MFI) was observed at the bead surface using a 1:20,000 dilution of anti-mouse-HRP (Fig. 2A). The same secondary antibody labeled with FITC gave a weak fluorescent signal even at a 200-fold higher concentration of antibody (43.4 ± 16 MFI) (Fig. 2B). Factoring in the difference in fluorescent signal and the antibody dilutions, the TSA method was approximately 500 fold more sensitive than the FITC method, confirming previous estimates (Bobrow et al., 1989; Speel et al., 1999).

To determine whether the TSA enhanced fluorescence was sufficient to detect individual KSHV virion particles by confocal microscopy, gradient purified biotin-labeled KSHV (bio-KSHV) virions were attached to poly-L-lysine coated slides. Bound virus particles were incubated with mouse anti-biotin IgG or mouse anti- KSHV virion envelope glycoprotein K8.1 followed by HRP conjugated anti-mouse IgG and TSA488. Individual virion particles were readily detected with antibodies to both biotin (Fig. 2C) and K8.1 (Fig. 2D). Analysis of the TSA-enhanced virion particle fluorescence using the Zeiss software revealed that the majority of the particles were uniform in size and not aggregated. Subsequently, DNP-KSHV virions were sequentially stained with the mouse anti-K8.1 and TSA488 (green) enhancement followed by rat anti-DNP and TSA647 (red) enhancement, as described in Materials and methods. Confocal microscopy revealed that the K8.1 glycoprotein staining co-localized with individual virion particles labeled with DNP (Fig. 2E and F), with a overlap coefficient of 0.9. The presence of K8.1 reactivity showed that the purified DNP-KSHV virions had intact envelopes, which correlated with the highly infectious nature of the hapten-labeled virus. Thus, TSA enhanced fluorescence was sufficient to detect virus particles by confocal analysis.

Localization of TSA enhanced fluorescence is highly specific and accurate

Since the correct localization of the TSA fluorescent product is dependent on tyramide deposition at the binding site of the HRP-labeled secondary antibody, we assessed the accuracy of TSA deposition by examining the specific localization of TSA fluorescence using monoclonal antibodies reacting with either cell surface $\beta 3$ integrin or two KSHV proteins, the ORF73 LANA and the ORF59 DNA polymerase processivity factor. Previous studies have shown that KSHV LANA localizes to discrete focal points in irregularly shaped bodies that associate with the border of heterochromatin in the nucleus of infected cells (Szekely et al., 1999), whereas ORF59 localizes diffusely across the nucleus (Chan et al., 1998). The antibody to $\beta 3$ integrin was used to delineate the cell surface. The monoclonal antibodies were visualized using

tyramides with different fluors and sequential TSA amplification reactions separated by intermediate peroxidase quenching steps to block any residual peroxidase activity and allow simultaneous detection of the different fluorescent signals. Short 10 min TSA amplification reactions were used since inaccurate TSA localization was observed using extended amplifications times of 30 min or longer (van Gijlswijk et al., 1996).

Vero cells were infected with KSHV for 24 h and then incubated with mouse anti-β3 integrin to label cell surface β3 integrin. The cells were fixed and the β3 integrin antibody was localized using anti-mouse IgG-HRP and TSA488 (green). Residual peroxidase activity was blocked by hydrogen peroxide and the cells were permeabilized and incubated with either rat anti-LANA or mouse anti-ORF59. Bound antibody was detected with species specific HRP conjugated secondary antibodies and TSA594 (red) enhancement. The cell nuclei were counterstained with TO-PRO 3 (blue), an ultrasensitive dye that detects double-stranded nucleic acid.

Confocal fluorescence microscopy revealed strong TSA enhanced labeling of the cell borders with the anti-β3 integrin antibody (Fig. 3A, green). The cell cytoplasm was unstained (black), and the nuclei stained with TO-PRO 3 (blue). TSA enhanced LANA fluorescence was restricted to specific focal points in the nucleus of the infected cells (Fig. 3A, red). The accuracy of the TSA localization was further shown at higher magnification where the TSA product was confined solely to the nucleus in discrete spots, even for spots directly adjacent to the nuclear membrane (Fig. 3B). The TSA localization matched the localization obtained previously with conventional FITC labeling with no obvious diffusion of tyramide within or outside of the nucleus. In Fig. 3C, the ORF 59 fluorescence (red) was distributed throughout the nucleus with a uniform pattern. Using the "profile" function of the Zeiss LSM Pascal software, the histogram showed that none of the ORF 59 TSA product had diffused into the cell cytoplasm, as all ORF59 pixels co-localized with TO-PRO 3 nuclear dye (Fig. 3D). This was particularly evident at the nuclear membrane edge where the histogram for both emissions overlapped (arrowhead). Additionally, the histogram revealed a simultaneous decrease in ORF 59 TSA (red) and nuclear DNA-associated TO-PRO (blue) fluorescence in the middle of the nucleus within the presumed site of the DNA-free nucleolus. Thus, the short 10 min TSA amplification resulted in a highly sensitive, specific and accurate localization of bound antibody probes.

Detection of cell surface bound KSHV comparing conventional FITC and TSA enhancement

To determine whether TSA enhanced fluorescence was capable of detecting hapten-labeled KSHV bound to cell surfaces, HT1080 cells were fixed with paraformaldehyde and incubated with DNP-KSHV. Paraformaldehyde fixation was used to preserve cytoskeletal structures involved in the initial virus interaction with the cell surface. Bound virus was detected using rat anti-DNP IgG and a secondary antibody coupled to either HRP or FITC. The FITC-labeled cells were visualized directly by confocal microscopy, while the HRP-labeled cells were further reacted with TSA488 to amplify the fluorescent signal. The conventional FITC antibody technique gave weak fluorescence with a punctate staining pattern for DNP-KSHV (Fig. 4A). In contrast, the TSA-enhanced technique gave a strong staining pattern with DNP-KSHV binding to distinct areas of the cells that were only weakly fluorescent with the FITC technique, including regions of cell substratum contact and intercellular junctions (Fig. 4B). KSHV binding was inhibited by heparin treatment (Fig. 4C), consistent with previous KSHV binding studies (Akula et al., 2001b).

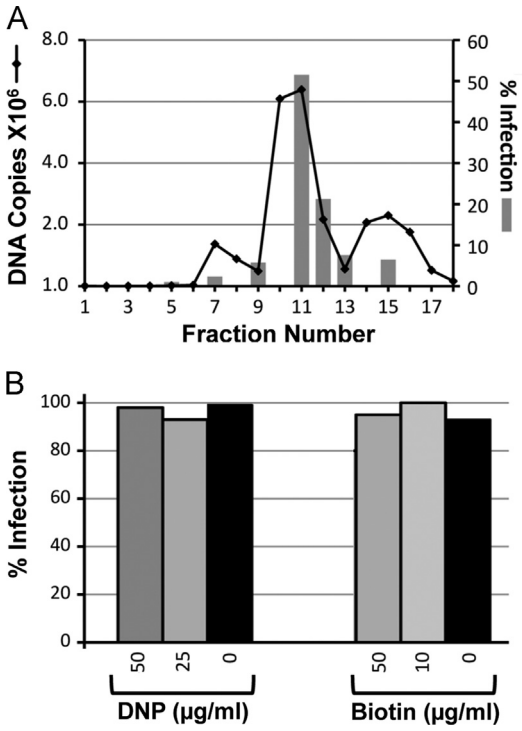

Fig. 1. Purification of hapten-labeled infectious KSHV. (A) KSHV virions were concentrated by centrifugation onto an Opti-Prep cushion, labeled with NHS-dinitrophenol (DNP) (50 µg/ml), and purified on a 10–40% Opti-Prep step gradient. Aliquots of gradient fractions were analyzed by qPCR to quantitate KSHV DNA. The infectivity of selected fractions (5, 7, 9, 11, 13, 15) was tested on Vero cells using an anti-LANA antibody to detect latently infected cells, as described in Materials and methods. (B) The effect of hapten incorporation on KSHV infectivity was assessed after labeling purified virus from the peak gradient fractions with different concentrations of DNP or biotin. The hapten-labeled virions were further purified on an Opti-Prep step gradient and tested for infectivity on Vero cells.

Hapten-labeled KSHV virions bind to specific cell surface domains

To further examine the cellular domains binding KSHV, confluent and sub-confluent HT1080 cell cultures were fixed and incubated with purified DNP-labeled KSHV, and bound virus was detected as above using the TSA method. The cell nuclei were stained with TO-PRO 3. As a control, HT1080 cells were incubated with a DNP-mock virus gradient fraction and stained using the identical protocol. In confluent cultures, DNP-KSHV strongly localized to distinct membrane regions, including intercellular junctions (Fig. 5A, arrowhead) and a supranuclear region (Fig. 5A, arrow), also shown in cross section (Fig. 5A, inset below). Large areas of the cell surface adjacent to the junctional regions showed little or no bound KSHV. In sub-confluent cultures, KSHV bound to supranuclear areas (Fig. 5B, chevron), intercellular junctions (Fig. 5B, double arrows) and dorsal cell surface microdomains (Fig. 5B and C, arrow) that were surrounded by adjacent virus-free membrane regions (Fig. 5B, indicated with "*"). The dorsal microdomains were numerous with significant size heterogeneity (Fig. 5B and C). In addition, there was a high level of KSHV binding to filopodia (Fig. 5B and C, arrowhead) and ruffled membranes (Fig. 5B and D, open arrow) at the cell margins and points of cell substratum contact. No cell-associated TSA488 signal was detected in HT1080 cells incubated with the DNP-labeled mock virus control (data not shown). KSHV binding studies on live cells at 4 °C gave equivalent results to the fixed cells, validating our findings.

The morphology of the KSHV binding domains was analyzed using Imaris 3D image analysis software. A region of interest (ROI)

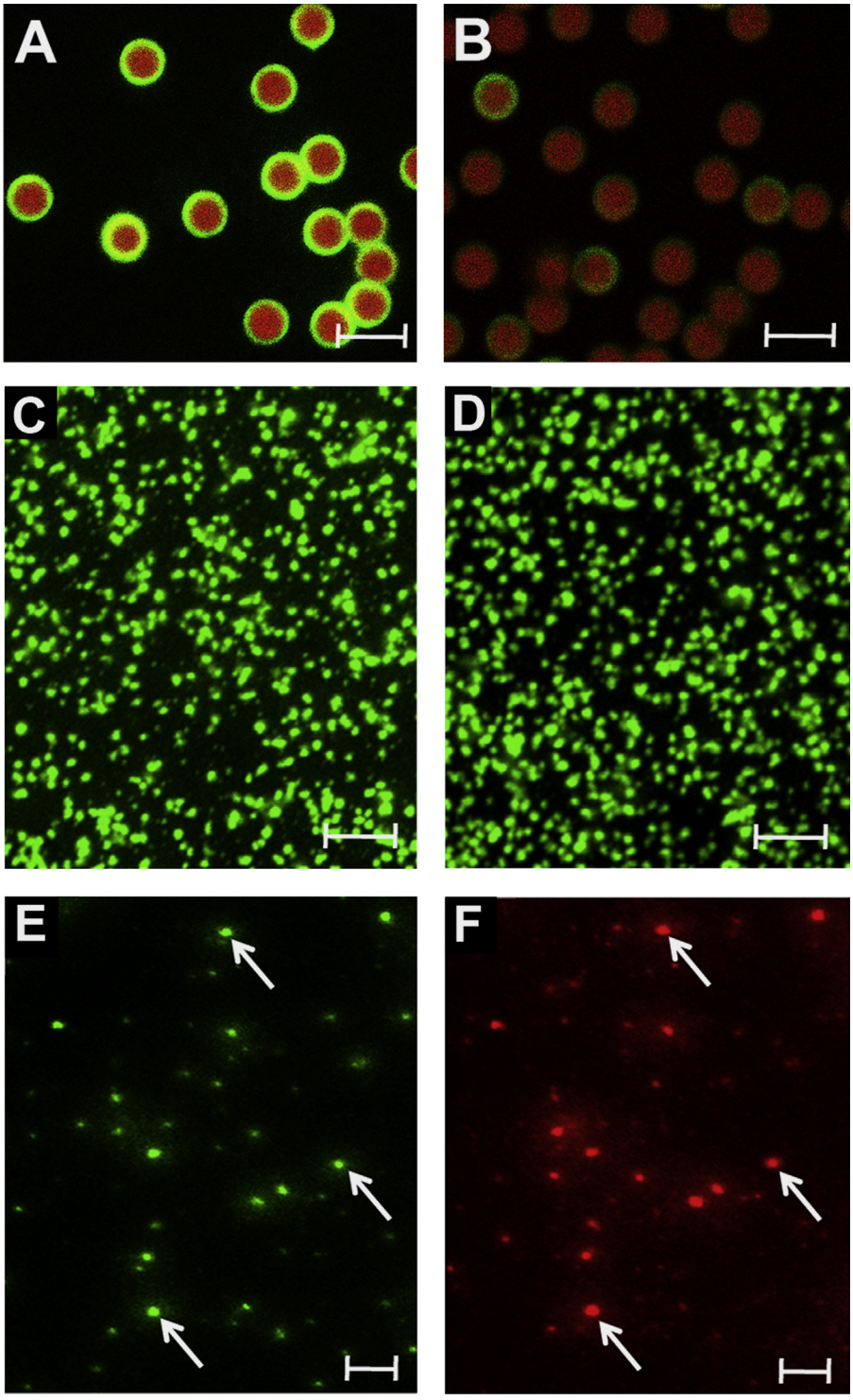

Fig. 2. Fluorescent signal enhancement by tyramide signal amplification (TSA) and use to detect labeled KSHV virions by confocal microscopy. (A) and (B) Fluorescent signal enhancement by the TSA method was assessed using an indirect immunoassay to detect biotinylated IgG coupled to magnetic beads. The beads were incubated with mouse anti-biotin IgG and dilutions of goat anti-mouse IgG conjugated with either (A) HRP (1:20,000) or (B) FITC (1:100). The HRP activity was detected using a 10 min amplification of TSA488. Fluorescence was visualized by confocal microscopy. (C)–(F) To determine if individual hapten-labeled KSHV virions could be detected by confocal microscopy using TSA enhancement, gradient purified biotin-KSHV (10 μg/ml) was immobilized on poly-L-lysine coated dishes and incubated with (C) goat anti-biotin-HRP antibody and TSA488 or (D) mouse anti-K8.1 antibody, which detects the K8.1 envelope glycoprotein of KSHV, and anti-mouse IgG-HRP, followed by TSA488 enhancement. (E) and (F) gradient-purified DNP-KSHV virions (10 μg/ml) were double stained with the mouse anti-K8.1 and TSA488, as above, followed by rat anti-DNP and TSA647. Individual virions (arrows) stained strongly for both K8.1 (green, 488 channel; (E)) and DNP (red, 647 channel; (F)) Bar = 5 μm.

within Fig. 5B (boxed area) was selected for 3D surface rendering (Fig. 6). The bound KSHV within the ROI is yellow while the nuclei are red, and the intercellular junction is marked with a dashed line. The dorsal surface KSHV-binding microdomains (open arrows), and supranuclear KSHV (chevron, Fig. 6A) are indicated. To better illustrate the restricted supranuclear KSHV domain, the rendering was enlarged and rotated (Fig. 6B; see arrows for orientation). The dorsal surface KSHV-binding microdomains outside of the ROI

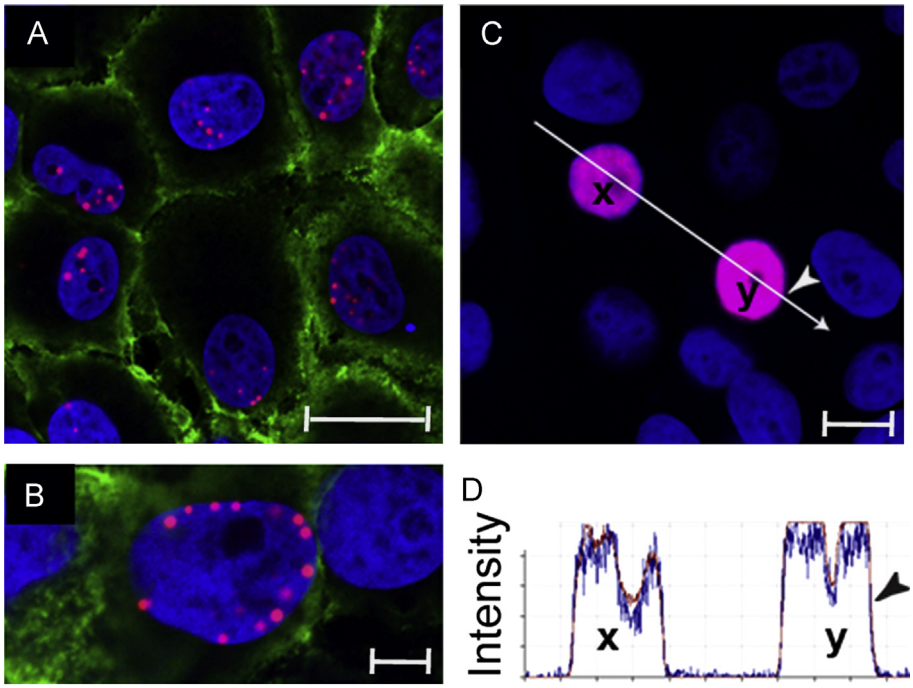

Fig. 3. Accuracy of TSA enhanced fluorescence. The accuracy of deposition of TSA fluorescence was determined by evaluating the localization of antibodies specific for cell surface β3 integrin and two KSHV proteins, ORF 73 LANA and ORF 59 DNA polymerase processivity factor. Vero cells were infected with KSHV for 24 h. (A) and (B) Infected cells were incubated with mouse anti-β3 integrin to label the cell surface. The cells were fixed and the β3 integrin antibody was localized using anti-mouse IgG-HRP with TSA488 enhancement (green). Subsequently, the cells were incubated with rat anti-LANA followed by anti-rat IgG-HRP with TSA594 enhancement (red). (B) High magnification micrograph showing LANA nuclear localization detail. (C) and (D) Infected cells were fixed and incubated with mouse anti-ORF59 followed by anti-mouse IgG-HRP with TSA594 enhancement (red). The nuclei of all cells were stained with TO-PRO 3 (blue) and fluorescence was examined by confocal microscopy. (D) A histogram of the anti-ORF59 (red) and TO-PRO 3 (blue) fluorescence along the white arrow in (C) across the two nuclei (x, y). The arrow crosses the apparent nucleolus of each cell, which appears as a region of decreased TO-PRO 3 stained DNA. An arrowhead denotes the limit of the nuclear membrane in (C) and (D). Bar A=20 μm, B=5 μm, C=10 μm.

appeared flat (Fig. 6B, star) while the rendering showed that the KSHV-binding sites were "raised" structures (open arrow, Fig. 6B). This is more clearly illustrated in Fig. 6C (XY view from above) and Fig. 6D, (XZ view from the side) showing distinct supranuclear KSHV-binding regions (chevron) and dorsal cell surface microdomains with a raised morphology extending 4–5 μm in the Z axis (Fig. 6D). The 3D rendering showed that the KSHV bound to the supranuclear region was clearly distinct from adjacent KSHV localized within dorsal surface microdomains (Fig. 6A–D).

We noted that the binding of KSHV was altered in a small percentage of cells in the culture. Some cells showed clear binding to the supranuclear region (chevron) and dorsal cell surface microdomains (arrow) (Fig. 7A, upper panel cell 1). The DNA of these cells reacted diffusely with TO-PRO 3 and was uniformly distributed over the whole cell nucleus with a clear nuclear margin (Fig. 7A, lower panel cell 1). 3D rendering showed that cell 1 had a flat and smooth nuclear membrane, characteristic of an interphase cell (Fig. 7B, top view) and (Fig. 7C, side view). In other cells, KSHV bound to extensive microvillar projections extending over the entire cell surface (Fig. 7A; cells 2 and 3). The TO-PRO 3 stained DNA in the nuclei of these cells showed obvious concentration and aggregation contrasting sharply with the DNA in interphase cell 1. Whereas the DNA in interphase cell 1 appeared diffuse and bordered by an intact nuclear membrane, the DNA in cell 3 was aggregated on a central line, characteristic of metaphase chromosomes in a mitotic cell lacking a defined nuclear membrane. 3D rendering of the TO-PRO 3 stain showed that cells 2 and 3 had raised nuclei with individual condensed chromosomes characteristic of mitotic cells (Fig. 7B and C; cells 2, cell 3 not shown). 3D rendering of DNP-KSHV (yellow) showed a high level of KSHV bound to surface projections on the mitotic cells 2 and 3 compared to the amount of KSHV bound to the small cell surface microdomains and supranuclear domain of interphase cell 1 (Fig. 7D). The 3D rendering of cell 3 was "sliced" to reveal the cell interior. This analysis demonstrated that the DNP-KSHV was bound continuously across the membrane of the mitotic cell 3 extending from the cell margins over the nucleus, which had an obvious raised morphology (Fig. 7D). The differences apparent in the DNA structure of cells 2 and 3 suggest that they are independently undergoing mitosis and are at different stages in the process.

Up-regulation of KSHV binding sites on mitotic cells

The morphology of the cells stained in Fig. 7 suggested that the DNP-KSHV was binding differentially to mitotic cells compared to interphase cells. As with propidium iodide, the amount of TO-PRO 3 incorporated into DNA has been used to distinguish G_0/G_1 cells (2n DNA content) from mitotic cells (4n) (Clevenger et al., 1985; Ploeger et al., 2008). To further investigate the increased KSHV binding on mitotic cells, Vero cells were treated with nocodazole to synchronize them in mitosis (Zieve et al., 1980). Vero cells were chosen because they are highly susceptible to KSHV infection and, unlike HT1080 cells, remain adherent following low dose nocodazole treatment allowing confocal analysis. The cells were fixed and incubated with DNP-KSHV and stained as in Fig. 7. The confocal micrograph of KSHV cell binding (Fig. 8A) showed that 24 h of nocodazole treatment (50 ng/ml) resulted in two cell populations that differentially bound DNP-KSHV and TO-PRO 3. One cell population stained strongly for both bound KSHV and nuclear TO-PRO 3 (Fig. 8A, B, closed arrows), while the other cell population stained weakly for both KSHV and TO-PRO 3 (Fig. 8A and B, open arrows). Fig. 8B shows only the TO-PRO 3 fluorescence which was converted to greyscale. The fluorescent pixels from

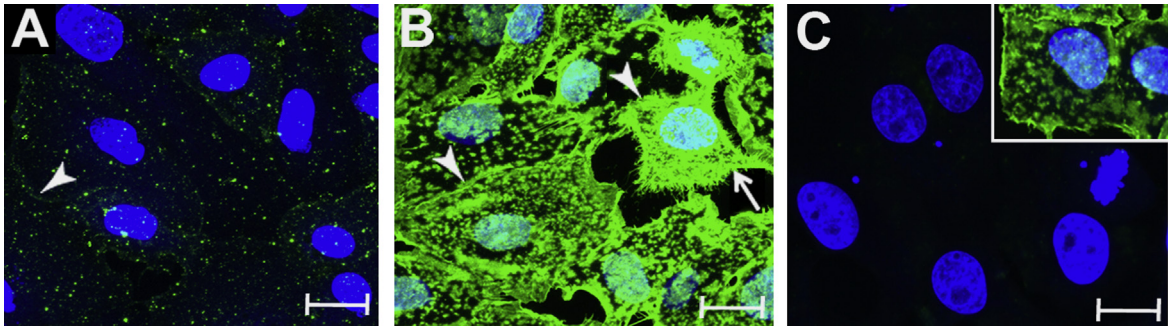

Fig. 4. Comparison of conventional FITC and TSA enhanced fluorescence detection of cell surface-bound KSHV. HT1080 cells were incubated with DNP-KSHV followed by rat anti-DNP IgG and a secondary anti-rat IgG antibody coupled to either (A) FITC or (B) HRP. The HRP-conjugates were detected with TSA488 enhancement. Arrowheads identify intercellular junctions, while the arrow indicates regions of cell substratum contact. To examine the specificity of binding, HT1080 cells were incubated with DNP-KSHV in the presence (C) or absence ((C), insert) of heparin, which is known to inhibit KSHV binding to cell surfaces, see text. Bar=20 μm.

both DNP-KSHV and TO-PRO 3 were quantitated for intact cells in the micrograph. The DNP-KSHV fluorescence gave mean pixel counts of 443 ± 28 and 20 ± 10 for the strongly and weakly staining cells, respectively, which were significantly different ($P < 0.0001$). The TO-PRO 3 fluorescence gave mean pixel counts of 119 ± 9 and 38 ± 16 (threshold=100) for the strongly and weakly staining cells respectively, which were also significantly different ($P=0.0005$). The DNP-KSHV and TO-PRO 3 fluorescence levels for each cell strongly correlated ($R^2=0.6202$; $P=0.0001$) (Fig. 8C). Although we could not identify metaphase chromosomes or condensed chromatin in these cells due to the nocodazole treatment, the TO-PRO 3 fluorescence data suggested that the weakly staining cells were in G_0/G_1 interphase ($2n$) while the strongly staining cells were mitotic as a result of the nocodazole block and had twice the DNA content ($4n$).

To confirm these findings, we incubated HT1080 cells with DNP-KSHV and TO-PRO 3 and examined the cell culture by confocal fluorescence microscopy to identify mitotic cells having characteristic metaphase chromosomes lined up in the cell center. Cells displaying intact nuclear membranes and diffuse and uniform TO-PRO 3 staining were defined as G_0/G_1 interphase (see cell 1, Fig. 7A, lower panel), while those cells displaying no nuclear membrane and TO-PRO 3 stained chromosomes on the metaphase plate were defined as mitotic (see cell 3, Fig. 7A, lower panel). A defined area (46 μm^2) of the nucleus was used to measure mean fluorescent intensity (MFI). As seen in Fig. 9A, the TO-PRO 3 fluorescence intensity of the G_0/G_1 cells showed a tight clustering with an MFI of 129 ± 5. In contrast, the cells identified as metaphase by microscopy showed approximately twice the DNA content with an average TO-PRO 3 MFI of 239 ± 6 and the difference was significant ($P < 0.0001$). The analysis of DNP-KSHV bound to the G_0/G_1 and metaphase cells was determined by counting anti-DNP/TSA488 pixels per cell with the minimal intensity threshold set at 150. The levels of KSHV fluorescence bound to the G_0/G_1 cells closely clustered with an average count of 170 ± 23 pixel/cell (Fig. 9B). In contrast, the levels of KSHV fluorescence bound to the metaphase cells clustered with an average count of 987 ± 83 pixel/cell, nearly six times the level of the G_0/G_1 cells ($P < 0.0001$). The DNP-KSHV and TO-PRO 3 fluorescence levels for each cell strongly correlated ($n=26$; $R^2=0.7761$; $P < 0.0001$) (Fig. 9C). These results demonstrate that the cell surface binding sites for KSHV were strongly up-regulated in mitotic cells in metaphase.

Discussion

In this study, we have characterized the cell surface structures initiating KSHV attachment using gradient purified infectious hapten-labeled virions visualized by confocal microscopy with a highly sensitive fluorescent signal enhancement procedure utilizing HRP-coupled antibodies and tyramides linked to different Alexa fluors. We determined that KSHV attachment sites were not randomly distributed on the cell membrane, but instead, were present in specific cellular domains, including actin-based filopodia, lamellipodia, ruffled membranes, microvilli and intercellular junctions. Similar binding specificities have been detected previously with individual viral envelope proteins (Birkmann et al., 2001; Hahn et al., 2009). KSHV also bound to isolated microdomains on the dorsal cell surface, which were heterogeneous in size with a variable distribution that depended on the degree of cell confluence and the stage of the cell cycle. These KSHV binding domains ranged from scarce on interphase cells to dense and continuous on mitotic cells. KSHV also bound to a region over the nucleus that was distinct from the microdomains in confluent and interphase cells. Due to the close proximity to the nuclear envelope, virus entry from this site could have a direct route to the nucleus for delivery of KSHV DNA during the infection process.

KSHV detection using labeled virus and TSA enhancement provided a highly sensitive approach to identify cell surface attachment domains. Specificity of virus binding was demonstrated using multiple approaches. The DNP-mock virus controls showed no cell binding, nor was there evidence of artifactual fluorescence derived from tyramide dispersion or sequential signal amplification steps using species specific HRP secondary antibodies. In addition we detected different distributions of bound KSHV on mitotic and interphase cells in the same experiment showing specificity of binding. Finally, we showed that virus binding is inhibited by heparin treatment, confirming the results of previous binding studies (Akula et al., 2001b; Birkmann et al., 2001).

The microdomains binding KSHV are larger than nanoscale lipid raft domains, and may represent larger “cross-linked” lipid raft cluster domains whose size and distribution is mediated by actin and myosin activity (Goswami et al., 2008; Mayor and Rao, 2004). Lipid rafts are known to contain some of the putative KSHV binding receptors, including the HS proteoglycans, syndecan-1 and syndecan-4 (Podyma-Inoue et al., 2012). However, the role of lipid rafts in KSHV attachment and entry is unclear and may be dependent on cell type, since KSHV infection of microvascular endothelial cells was inhibited by drugs that disrupt lipid rafts (Chakraborty et al., 2011; Raghu et al., 2007), while infection of vascular endothelial cells (Greene and Gao, 2009) and human foreskin fibroblasts (Akula et al., 2003) was unaffected.

Previously, we identified the integrin $\alpha v\beta 3$ as an entry receptor for KSHV. We showed that purified $\alpha v\beta 3$ integrin specifically bound to KSHV virions, recognizing the RGD motif of KSHV virion glycoprotein B, and anti-$\alpha v\beta 3$ antibodies and RGD peptides

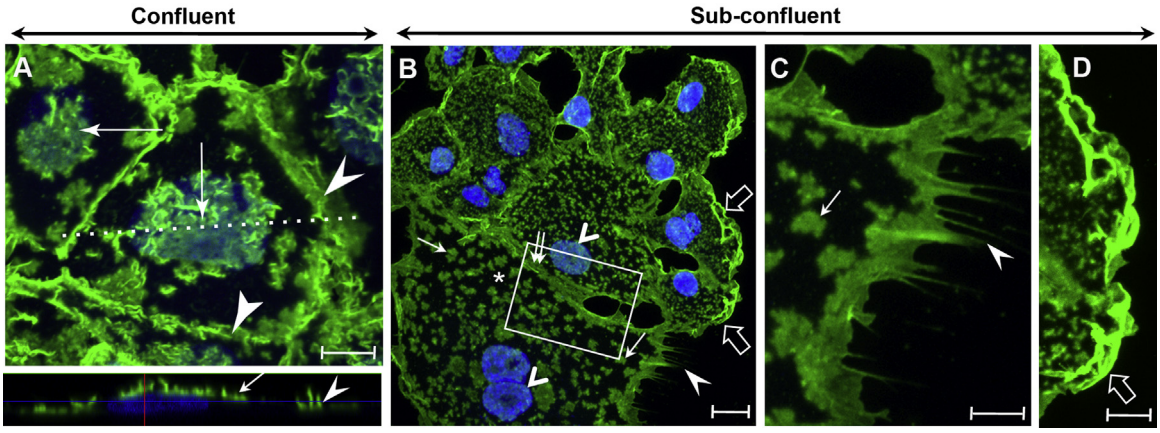

Fig. 5. Analysis of cell surface domains binding KSHV. Confluent (A) or sub-confluent ((B)–(D)) HT1080 cultures were fixed and incubated with DNP-KSHV. KSHV was detected with anti-DNP (TSA488, green) and nuclei were stained with TO-PRO 3 (blue). In confluent cultures, KSHV bound preferentially to intercellular junctions ((A), arrowhead) and to membrane areas directly over the nucleus ((A), arrow). Upper panel=(x, y) top view. The dotted line indicates the position of the (x, z) side view in the adjacent panel below, which shows supranuclear KSHV (arrow) and junctional KSHV (arrowhead). In sub-confluent cultures, KSHV binding sites on the dorsal cell surface were heterogeneous in size and number, forming distinct microdomains ((B) and (C), arrows) separated by membrane areas lacking KSHV ((B), indicated by "*"). KSHV also localized to supranuclear domains ((B), chevron), intercellular junctions ((B), double arrow), filopodia ((B) and (C), arrowheads) and ruffled membranes at the cell margin ((B) and (D)), open arrows). Bar in (A) (C) and (D)=10 μm; Bar in B=20 μm.

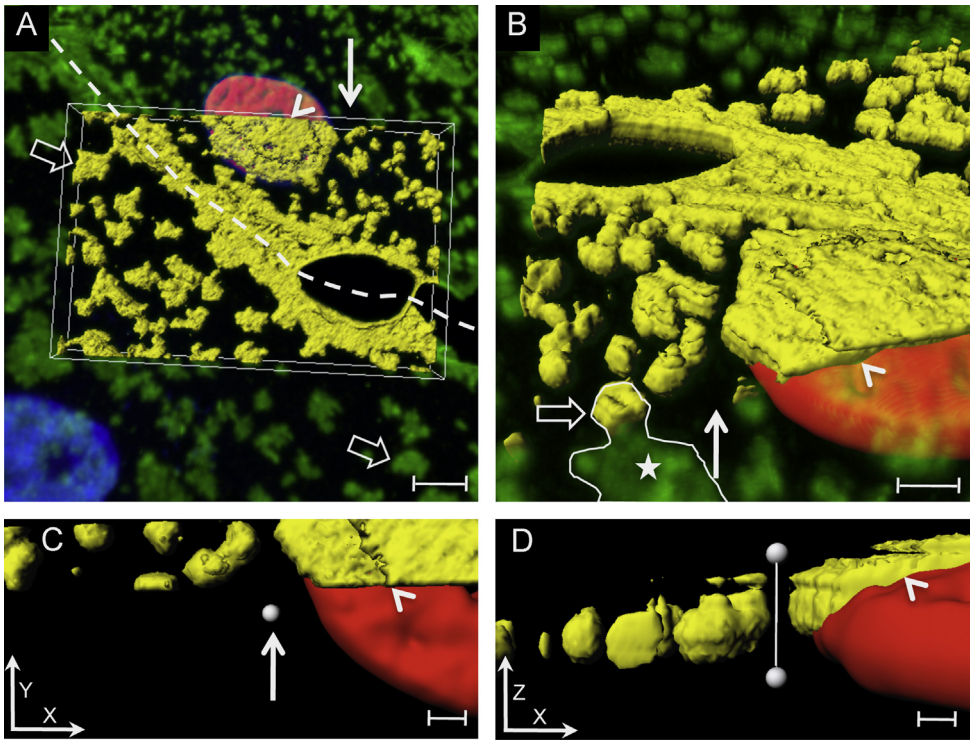

Fig. 6. 3D surface rendering of KSHV supranuclear and cell surface microdomains. A region of interest (ROI) from Fig. 5B (box) was selected for 3D surface rendering with surrounding fluorescence (green) in 2D for comparison. KSHV and nuclear fluorescence within the ROI were converted to yellow and red, respectively. The rendering in (A) was rotated 180°, zoomed and tilted in (B). A vertical arrow is an orientation point. Distinct KSHV binding to intercellular junctions (dashed line), supranuclear domain (chevron), and individual cell surface microdomains (open arrow) are visible (A) and (B). The ROI bisects the red nucleus to illustrate the distinct position of KSHV directly over the nucleus. The original confocal projection appears flat without structural detail (e.g. (B) indicated by "*", green), while the rendered image of the microdomain edge ((B), open arrow, yellow) shows the complex raised morphology of the KSHV binding domain. (C)) (x, y) overhead view and (D)) (x, z) side views show that the KSHV binding (chevron) was confined to the supranuclear surface, while the cell surface microdomains have a raised morphology. The distance between the white spheres is 5.6 μm (D). Bar in A=10 μm; B=5 μm; C, D=2 μm.

blocked KSHV infection (Garrigues et al., 2008). Interestingly, studies have shown that $\alpha v\beta 3$ integrins are up-regulated on the cell surface during mitosis (Anilkumar et al., 1996; Fender et al., 2008). In this latter study using adenovirus, which contains a cell attachment domain that interacts with both HS-proteoglycans and $\alpha v\beta 3$ integrin through multiple RGD motifs, they demonstrated that HS-proteoglycans are mainly responsible for virus attachment allowing interaction with $\alpha v\beta 3$ integrin to induce internalization. However, $\alpha v\beta 3$ integrin mediated virus binding and entry in HS-proteoglycan deficient cells. They also detected

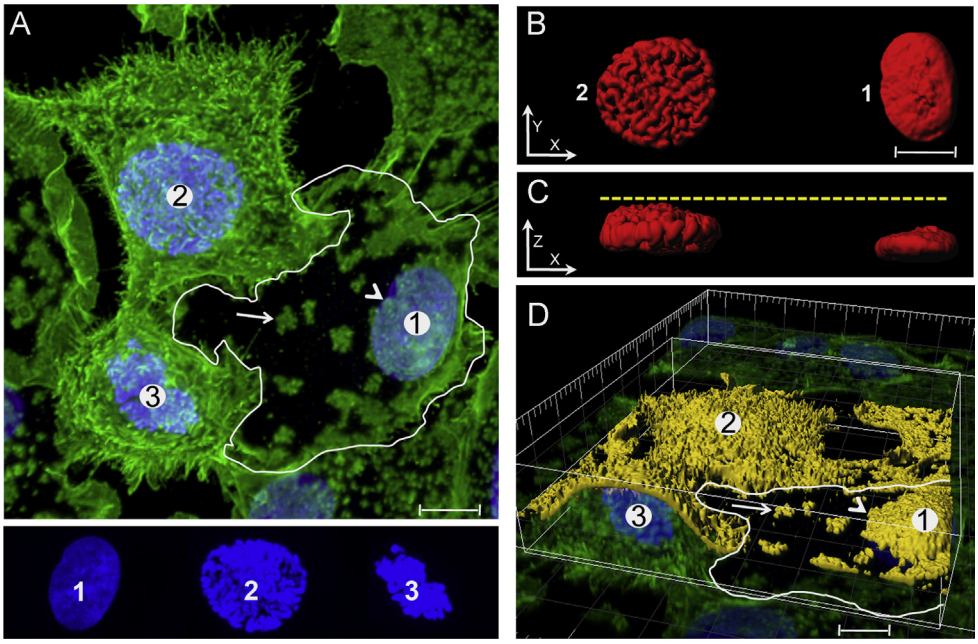

Fig. 7. Enhanced KSHV binding to mitotic cells. HT1080 cells were incubated with DNP-KSHV and TO-PRO 3 (described in Fig. 5) to characterize the KSHV binding sites (green) on three cells showing differential KSHV binding. (A) Distinct KSHV binding to supranuclear (chevron) and sparse dorsal cell surface microdomains (arrow) is shown for cell 1 (Upper panel, outlined). KSHV bound to cell surface microvilli protruding from the entire dorsal surface on cells 2 and 3. TO-PRO 3 stained nuclei for cells 1, 2, and 3 are shown in the lower panel to demonstrate the diffuse DNA stain of cell 1 (interphase) compared to the condensed DNA in cells 2 and 3. Based on the chromosome morphology, cell 3 appears to be in metaphase. (B) overhead and (C) side view surface renderings of nuclei in cells 1 and 2 are shown to illustrate the distinct condensed chromatin and raised morphology of the nucleus of cell 2 compared to the flat and smooth morphology of cell 1. Cell 1 has an intact nuclear membrane and therefore is a G_0/G_1 interphase cell while cells 2 and 3 have condensed chromatin characteristic of mitotic cells. (D) A surface rendering of a ROI in panel A is shown with bound KSHV (yellow). The mitotic cells 2 and 3 had high levels of KSHV bound extensively to microvilli across the entire cell surface, whereas the interphase cell 1 had KSHV bound to sparse dorsal surface microdomains (arrow) and supranuclear region (chevron). Bars = 10 μm.

enhanced adenovirus binding to mitotic cells and determined that the enhanced binding to mitotic cells was mediated by an up-regulation of $\alpha v\beta 3$ integrin on the cell surface. These studies suggest that the increased binding of KSHV to mitotic cells that we detected may be due to $\alpha v\beta 3$ interactions. We have previously seen that mitotic cells are more susceptible to KSHV infection, and are currently exploring the role of $\alpha v\beta 3$ in KSHV binding and entry and its presence in the KSHV binding domains identified in this study.

Materials and methods

Cell lines

The human HT1080 fibrosarcoma cell line was a gift of Dr. W. Carter. African green monkey Vero cells were from the American Type Tissue Culture. HT 1080 and Vero cells were maintained in DMEM containing 10% fetal bovine serum (FBS). BCBL-1 cells latently infected with KSHV (Renne et al., 1996), were cultured in RPMI complete medium with 10% FBS, 100 U/ml penicillin, 100 μg/ml streptomycin, 1.0 mM HEPES, and 0.01% 2-mercaptoethanol at 37 °C.

Immunological reagents

The mouse monoclonal antibody against $\beta 3$ integrin (clone B3A) was purchased from Chemicon. Other antibody reagents included: goat anti-mouse IgG-HRP, goat anti-mouse IgG-FITC, goat anti-rat IgG-HRP, non-immune mouse IgG, and mouse anti-biotin IgG (Jackson Immunochemicals); mouse anti-K8.1A (clone 2A3), rat anti-LANA (clone LN53), and mouse anti-ORF 59 (clone 11D1) (Advanced Biotechnologies); goat anti-biotin-HRP, non-immune goat serum, biotinylated goat IgG (Sigma); monoclonal rat anti-DNP (clone LO-DNP-2; Invitrogen). Other reagents include: TSA-488, TSA-594, TSA-647, TO-PRO 3, and SlowFade (Invitrogen).

KSHV labeling and purification

KSHV virions from culture supernatants of TPA-treated BCBL cells were concentrated 200-fold by centrifugation onto an Opti-Prep cushion, as described previously (Garrigues et al., 2008). In some experiments, aliquots of concentrated KSHV were labeled with NHS-POE4-biotin (10–50 μg/ml) or NHS-dinitrophenol (DNP) (10–50 μg/ml) and purified by centrifugation on a 20%, 25%, 30%, and 40% Opti-Prep step gradient. Fractions were collected from the top of the gradient using a BioComp gradient station (BioComp Instruments, Inc., New Brunswick, Canada). KSHV DNA from each fraction was quantified by real time PCR to detect *v*-cyclin and infectivity of labeled virus was determined (see below). As a labeling control, fractions from a mock virus gradient were similarly labeled with DNP.

KSHV infection

Vero cells were infected with either unlabeled KSHV or various fractions of labeled (DNP or biotin) KSHV for 3 h at 37 °C, washed, and incubated for an additional 24 h. In some experiments, the infected cells were then cooled to 4 °C and incubated with anti-$\beta 3$ antibody for 1 h at 4 °C to detect cell surface $\alpha v\beta 3$ integrin. The cultures were then fixed with 4% paraformaldehyde (PF) in PHEM/sucrose (60 mM PIPES, 25 mM Hepes, 10 mM EGTA, 2 mM $MgCl_2$, 4% sucrose) for 30 min at 37 °C. Free aldehydes were quenched with 50 mM NH_4Cl and the cells were permeabilized with 0.5% NP-40/0.2% Tween 20. Endogenous peroxidase activity was inhibited with 3% H_2O_2. The cells were incubated with 10% normal goat

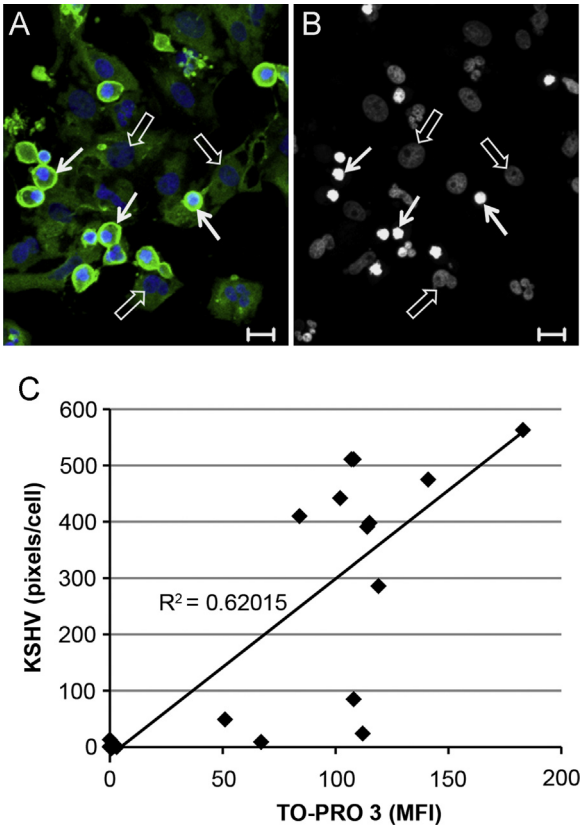

Fig. 8. KSHV binding sites are up-regulated on mitotic Vero cells after nocodazole treatment. Vero cells were treated with nocodazole (50 ng/ml) for 24 h to block the cell cycle at mitosis. The cells were fixed and incubated with DNP-KSHV and TO-PRO 3 as in Fig. 5. (A) Micrograph of merged DNP-KSHV (green) and TO-PRO 3 (blue) fluorescence. (B) TO-PRO 3 fluorescence alone (greyscale). Solid and open arrows indicate cells with high and low levels of DNP-KSHV and TO-PRO 3 staining, respectively. (C) DNP-KSHV and TO-PRO 3 fluorescent pixels were counted for each cell and the correlation was determined using Pearson's correlation analysis. $n=24$; $R^2=0.6202$; $P=0.0001$ (two-tailed, significant at the 0.05 level). Bar=20 μm.

serum (NGS) followed by 10% milk containing 1% NGS (blotto/NGS) to block non-specific binding. For those cultures incubated with anti-β3, the integrin was detected with anti-mouse IgG-HRP followed by a 10 min TSA amplification with TSA488. Residual peroxidase activity was quenched with 1% H_2O_2 for 15 min. The cells were then incubated with either rat anti-LANA monoclonal antibody LN53 (1:500) or mouse anti-ORF 59 (1:500) to detect KSHV infected cells. The cells were washed and bound antibody was detected with a goat anti-rat or mouse IgG-HRP (1:100) and TSA488 or TSA594 in $\alpha v\beta 3$ integrin colocalization experiments. The nuclei were stained with TO-PRO 3. The cells were analyzed by confocal microscopy and the percent of cells expressing nuclear LANA was determined manually (100–200 cells counted/group).

Sensitivity of tyramide signal amplification (TSA)

NeutrAvidin (Pierce) was coupled to Dynabeads, as described previously (Garrigues et al., 2008). Biotinylated goat IgG was immobilized on NeutrAvidin beads (0.04 μg IgG/4.2 mg beads). The beads were attached to poly L-lysine coated slides and subsequently fixed with 8% paraformaldehyde. The immobilized beads were blocked with blotto/NGS. The biotinylated goat IgG was detected with mouse anti-biotin (1:100) followed by anti-mouse IgG-HRP (1:20,000) and TSA488 or, for comparison, the same anti-mouse IgG conjugated to FITC (1:100) using the same laser settings.

Accuracy of TSA localization

Vero cells were infected with unlabeled KSHV. In some experiments, infected cells were fixed, quenched, blocked, and incubated with a mouse anti-ORF 59 and TSA594 as above. In other experiments, live infected cells were double stained for KSHV LANA and cell surface $\alpha v\beta 3$ integrin, using the mouse anti-β3 antibody and TSA488, followed by the rat anti-LANA antibody and TSA594 as above. The accuracy of the TSA localization was assessed by comparing the distribution of the LANA and ORF 59 TSA fluorescence relative to the TO-PRO 3 stained nuclei using the profile function of the Zeiss LSM 4.2 software.

Detection of KSHV virion particles by TSA-enhanced immunofluorescence

Purified KSHV virions labeled with 10 μg/ml of either biotin or DNP were immobilized on poly-L-lysine coated slides and stained with either goat anti-biotin-HRP (1:100) or anti-K8.1 (1:100) and TSA 488 as above. To assess virion integrity, individual virion particles were double stained with mouse anti-K8.1 (1:100) and TSA488, followed by rat anti-DNP and TSA647. The co-localization of both TSA fluorescent signals within individual KSHV particles was determined by confocal microscopy to evaluate virus envelope integrity.

Localization of cell-bound KSHV

HT1080 cells were seeded at 1×10^4 cells per well (confluent) or 4×10^3 cells per well (sub-confluent) and cultured for 24–48 h. Vero cells were treated with nocodazole (50 ng/ml) for 24 h to block the cell cycle at mitosis. The cells were fixed, quenched, and blocked as above. The cells were washed with DMEM and incubated for 3 h with gradient-purified DNP-KSHV (10 μg/ml DNP) at a concentration of 1000 viral genomes/cell to be able to saturate the virus binding sites. The cells were then washed, fixed and blocked. Bound DNP-KSHV was detected with monoclonal rat anti-DNP diluted 1:100 in blotto/NGS followed by goat anti-rat IgG-HRP (1:100) and TSA488. In some experiments, bound virus was detected with the same secondary antibody conjugated to FITC to compare the sensitivity of the TSA and FITC methods. Inhibition of virus binding by heparin was done as above except DNP-KSHV was pretreated with heparin (10 μg/ml) prior to and during overnight virus incubation.

Confocal microscopy

Confocal images were generated on an LSM 5 Pascal system (Zeiss) equipped with 40×1.3 NA and 63×1.4 NA objectives. Image maximum projections were compiled from Z-stacks of 30–50 sections with intervals ranging from 0.3–0.4 μm and a Z-distance of 10–14 μm. Confocal images were deconvolved using AutoQuant × AutoDeblur Gold CF (Media Cybernetics, Inc.). Three-dimensional surface renderings of deconvolved images were done with Imaris 7.3 (Bitplane AG). For the analysis of KSHV binding to HT1080 mitotic cells, DNA content was estimated by comparing TO-PRO 3 fluorescent intensity of a 46 μm^2 area over G_0/G_1 cells with intact nuclear membranes compared to the same area over metaphase chromosomes found at the cell center with no visible nuclear membrane. For experiments using nocodazole, the TO-PRO 3 intensity was determined for the whole cell since distinct mitotic chromosomes in metaphase were not resolved. The LSM software was used to measure fluorescent intensity. To measure

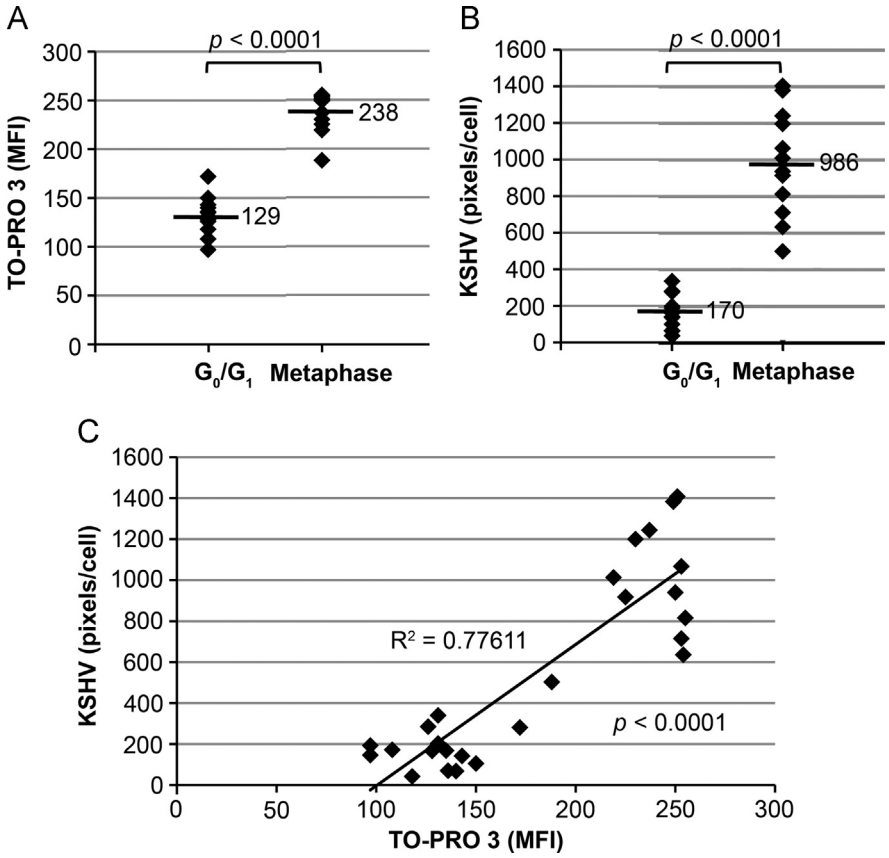

Fig. 9. KSHV binding sites are upregulated on mitotic HT1080 cells in metaphase. To quantitate the KSHV binding sites on interphase and mitotic cells, HT1080 cells were incubated with DNP-KSHV and TO-PRO 3 as in Fig. 8. The cells were examined by confocal microscopy and segregated into two groups based on TO-PRO 3 staining. G_0/G_1 interphase cells: intact nuclear membrane and diffuse TO-PRO 3 stained DNA and metaphase cells: lacking a defined nuclear membrane with visible condensed chromatin organized at the cell center. For each cell, (A) the DNA content was determined as a mean fluorescent intensity (MFI) of the TO-PRO 3 fluorescence within a defined 46 μm^2 area of the nucleus, and (B) the amount of cell-bound DNP-KSHV was determined as DNP-KSHV pixels/cell. (C) The correlation between the levels of DNP-KSHV and TO-PRO 3 stained DNA was determined using Pearson's correlation analysis. $n=26$, $R^2=0.7761$, $P<0.0001$ (two-tailed, significant at the 0.05 level).

bound DNP-KSHV, cell boundaries were determined and marked based on a combination of morphology and KSHV fluorescence. The number of fluorescent pixels/cell for the anti-DNP antibody was determined using the histogram function of the LSM software with the threshold set at 150.

Data analysis

The GraphPad Prism software was used for statistical analysis. The unpaired *t* test (two-tailed) was used to compare fluorescent pixel levels in the different cell populations. The Pearson's correlation analysis was employed to determine the correlation between fluorescent pixel levels.

Acknowledgments

We acknowledge W. Carter for the HT1080 cell line. This work was supported by the National Institute for Dental and Craniofacial Research (NIDCR) of the National Institutes of Health under awards number DEO18927 and DE021954. The content is solely the responsibility of the authors and does not necessarily represent official views of the National Institutes of Health.

References

Akula, S.M., Naranatt, P.P., Walia, N.S., Wang, F.Z., Fegley, B., Chandran, B., 2003. Kaposi's sarcoma-associated herpesvirus (human herpesvirus 8) infection of human fibroblast cells occurs through endocytosis. J. Virol. 77, 7978–7990.

Akula, S.M., Pramod, N.P., Wang, F.Z., Chandran, B., 2001a. Human herpesvirus 8 envelope-associated glycoprotein B interacts with heparan sulfate-like moieties. Virology 284, 235–249.

Akula, S.M., Pramod, N.P., Wang, F.Z., Chandran, B., 2002. Integrin alpha3beta1 (CD 49c/29) is a cellular receptor for Kaposi's sarcoma-associated herpesvirus (KSHV/HHV-8) entry into the target cells. Cell 108, 407–419.

Akula, S.M., Wang, F.Z., Vieira, J., Chandran, B., 2001b. Human herpesvirus 8 interaction with target cells involves heparan sulfate. Virology 282, 245–255.

Anilkumar, N., Bhattacharya, A.K., Manogaran, P.S., Pande, G., 1996. Modulation of alpha 5 beta 1 and alpha V beta 3 integrins on the cell surface during mitosis. J. Cell Biochem. 61, 338–349.

Balogh, A., Pap, M., Marko, L., Koloszar, I., Csatary, L.K., Szeberenyi, J., 2011. A simple fluorescent labeling technique to study virus adsorption in Newcastle disease virus infected cells. Enzyme Microb. Technol. 49, 255–259.

Bechtel, J.T., Liang, Y., Hvidding, J., Ganem, D., 2003. Host range of Kaposi's sarcoma-associated herpesvirus in cultured cells. J. Virol. 77, 6474–6481.

Birkmann, A., Mahr, K., Ensser, A., Yaguboglu, S., Titgemeyer, F., Fleckenstein, B., Neipel, F., 2001. Cell surface heparan sulfate is a receptor for human herpesvirus 8 and interacts with envelope glycoprotein K8.1. J. Virol. 75, 11583–11593.

Bobrow, M.N., Harris, T.D., Shaughnessy, K.J., Litt, G.J., 1989. Catalyzed reporter deposition, a novel method of signal amplification. Application to immunoassays. J. Immunol. Methods 125, 279–285.

Chakraborty, S., Veettil, M., Sadagopan, S., Paudel, N., Chandran, B., 2011. c-Cbl-mediated selective virus-receptor translocations into lipid rafts regulate productive Kaposi's sarcoma-associated herpesvirus infection in endothelial cells. J. Virol. 85, 12410–12430.

Chan, S.R., Bloomer, C., Chandran, B., 1998. Identification and characterization of human herpesvirus-8 lytic cycle-associated ORF 59 protein and the encoding cDNA by monoclonal antibody. Virology 240, 118–126.

Clevenger, C.V., Bauer, K.D., Epstein, A.L., 1985. A method for simultaneous nuclear immunofluorescence and DNA content quantitation using monoclonal antibodies and flow cytometry. Cytometry 6, 208–214.

Fender, P., Schoehn, G., Perron-Sierra, F., Tucker, G.C., Lortat-Jacob, H., 2008. Adenovirus dodecahedron cell attachment and entry are mediated by heparan sulfate and integrins and vary along the cell cycle. Virology 371, 155–164.

Ganem, D., 2006. KSHV infection and the pathogenesis of Kaposi's sarcoma. Annu. Rev. Pathol. 1, 273–296.

Garrigues, H.J., Rubinchikova, Y.E., Dipersio, C.M., Rose, T.M., 2008. Integrin alphaVbeta3 binds to the RGD motif of glycoprotein B of Kaposi's sarcoma-associated herpesvirus and functions as an RGD-dependent entry receptor. J. Virol. 82, 1570–1580.

Goswami, D., Gowrishankar, K., Bilgrami, S., Ghosh, S., Raghupathy, R., Chadda, R., Vishwakarma, R., Rao, M., Mayor, S., 2008. Nanoclusters of GPI-anchored proteins are formed by cortical actin-driven activity. Cell 135, 1085–1097.

Greene, W., Gao, S.J., 2009. Actin dynamics regulate multiple endosomal steps during Kaposi's sarcoma-associated herpesvirus entry and trafficking in endothelial cells. PLoS Pathog. 5, e1000512.

Hahn, A., Birkmann, A., Wies, E., Dorer, D., Mahr, K., Sturzl, M., Titgemeyer, F., Neipel, F., 2009. Kaposi's sarcoma-associated herpesvirus gH/gL: glycoprotein export and interaction with cellular receptors. J. Virol. 83, 396–407.

Hahn, A.S., Kaufmann, J.K., Wies, E., Naschberger, E., Panteleev-Ivlev, J., Schmidt, K., Holzer, A., Schmidt, M., Chen, J., Konig, S., Ensser, A., Myoung, J., Brockmeyer, N. H., Sturzl, M., Fleckenstein, B., Neipel, F., 2012. The ephrin receptor tyrosine kinase A2 is a cellular receptor for Kaposi's sarcoma-associated herpesvirus. Nat. Med. 18, 961–966.

Jarousse, N., Chandran, B., Coscoy, L., 2008. Lack of heparan sulfate expression in B-cell lines: implications for Kaposi's sarcoma-associated herpesvirus and murine gammaherpesvirus 68 infections. J. Virol. 82, 12591–12597.

Kaleeba, J.A., Berger, E.A., 2006. Kaposi's sarcoma-associated herpesvirus fusion-entry receptor: cystine transporter xCT. Science 311, 1921–1924.

Lagunoff, M., Bechtel, J., Venetsanakos, E., Roy, A.M., Abbey, N., Herndier, B., McMahon, M., Ganem, D., 2002. De novo infection and serial transmission of Kaposi's sarcoma-associated herpesvirus in cultured endothelial cells. J. Virol. 76, 2440–2448.

Liu, J., Thorp, S.C., 2002. Cell surface heparan sulfate and its roles in assisting viral infections. Med. Res. Rev. 22, 1–25.

Mark, L., Lee, W.H., Spiller, O.B., Villoutreix, B.O., Blom, A.M., 2006. The Kaposi's sarcoma-associated herpesvirus complement control protein (KCP) binds to heparin and cell surfaces via positively charged amino acids in CCP1-2. Mol. Immunol. 43, 1665–1675.

Mayor, S., Rao, M., 2004. Rafts: scale-dependent, active lipid organization at the cell surface. Traffic 5, 231–240.

Ploeger, L.S., Dullens, H.F., Huisman, A., van Diest, P.J., 2008. Fluorescent stains for quantification of DNA by confocal laser scanning microscopy in 3-D. Biotech. Histochem. 83, 63–69.

Podyma-Inoue, K.A., Hara-Yokoyama, M., Shinomura, T., Kimura, T., Yanagishita, M., 2012. Syndecans reside in sphingomyelin-enriched low-density fractions of the plasma membrane isolated from a parathyroid cell line. PLoS One 7, e32351.

Raghu, H., Sharma-Walia, N., Veettil, M.V., Sadagopan, S., Caballero, A., Sivakumar, R., Varga, L., Bottero, V., Chandran, B., 2007. Lipid rafts of primary endothelial cells are essential for Kaposi's sarcoma-associated herpesvirus/human herpesvirus 8-induced phosphatidylinositol 3-kinase and RhoA-GTPases critical for microtubule dynamics and nuclear delivery of viral DNA but dispensable for binding and entry. J. Virol. 81, 7941–7959.

Rappocciolo, G., Hensler, H.R., Jais, M., Reinhart, T.A., Pegu, A., Jenkins, F.J., Rinaldo, C.R., 2008. Human herpesvirus 8 infects and replicates in primary cultures of activated B lymphocytes through DC-SIGN. J. Virol. 82, 4793–4806.

Rappocciolo, G., Jenkins, F.J., Hensler, H.R., Piazza, P., Jais, M., Borowski, L., Watkins, S.C., Rinaldo , C.R., 2006. DC-SIGN is a receptor for human herpesvirus 8 on dendritic cells and macrophages. J. Immunol. 176, 1741–1749.

Renne, R., Zhong, W., Herndier, B., McGrath, M., Abbey, N., Kedes, D., Ganem, D., 1996. Lytic growth of Kaposi's sarcoma-associated herpesvirus (human herpesvirus 8) in culture. Nat. Med. 2, 342–346.

Speel, E.J., Hopman, A.H., Komminoth, P., 1999. Amplification methods to increase the sensitivity of in situ hybridization: play card(s). J. Histochem. Cytochem. 47, 281–288.

Szekely, L., Kiss, C., Mattsson, K., Kashuba, E., Pokrovskaja, K., Juhasz, A., Holmvall, P., Klein, G., 1999. Human herpesvirus-8-encoded LNA-1 accumulates in heterochromatin- associated nuclear bodies. J. Gen. Virol. 80 (Pt 11), 2889–2900.

van Gijlswijk, R.P., Wiegant, J., Raap, A.K., Tanke, H.J., 1996. Improved localization of fluorescent tyramides for fluorescence in situ hybridization using dextran sulfate and polyvinyl alcohol. J. Histochem. Cytochem. 44, 389–392.

Veettil, M.V., Sadagopan, S., Sharma-Walia, N., Wang, F.Z., Raghu, H., Varga, L., Chandran, B., 2008. Kaposi's sarcoma-associated herpesvirus forms a multimolecular complex of integrins (alphaVbeta5, alphaVbeta3, and alpha3beta1) and CD98-xCT during infection of human dermal microvascular endothelial cells, and CD98-xCT is essential for the postentry stage of infection. J. Virol. 82, 12126–12144.

Wang, F.Z., Akula, S.M., Pramod, N.P., Zeng, L., Chandran, B., 2001. Human herpesvirus 8 envelope glycoprotein K8.1A interaction with the target cells involves heparan sulfate. J. Virol. 75, 7517–7527.

Whitt, M.A., Mire, C.E., 2011. Utilization of fluorescently-labeled tetracysteine-tagged proteins to study virus entry by live cell microscopy. Methods 55, 127–136.

Zieve, G.W., Turnbull, D., Mullins, J.M., McIntosh, J.R., 1980. Production of large numbers of mitotic mammalian cells by use of the reversible microtubule inhibitor nocodazole. Nocodazole accumulated mitotic cells. Exp. Cell. Res. 126, 397–405.